

Development and Characterization of the Helicon Plasma Thruster Prototype HPT05M

IEPC-2019-596

*Presented at the 36th International Electric Propulsion Conference
University of Vienna, Austria
September 15-20, 2019*

J. Navarro-Cavallé*, M. Wijnen†, P. Fajardo‡ and E. Ahedo§

Equipo de plasmas y propulsión eléctrica (EP2), Universidad Carlos III de Madrid, Leganés, 28911, Spain

V. Gómez¶, A. Giménez||, M. Ruiz**,

Sener Aeroespacial S.A., Las Arenas, Bizcaia, 48930, Spain

This paper begins with a brief review of the HPT technology development within the fruitful joint-venture between UC3M and SENER Aeroespacial. Starting from the first experimental platform, rated at 1 kW, passing through different modifications of the initial breadboard, until the last design, scaled down to 450 W of nominal power, called the HPT05M prototype. The experimental methodology to assess the thrust capabilities of the HPT05M, based on the plasma plume inspection, is discussed and accompanied by the latest results, which show a promising thrust efficiency around the 10 %. Lastly, the main specifications for the new design, an engineering model of the former platform, called HPT03, are presented.

Nomenclature

α	= angle between the probe rotary arm and the thruster axis line
α_d	= beam divergence
B	= magnetic field.
$d\alpha$	= differential of α .
D	= chamber diameter.
e	= electron singly charge.
e_i	= ion kinetic energy flux.
f_i	= Ion Energy Distribution Function (IEDF).
F	= thrust.
I_b	= ion beam current.
I_{sp}	= specific impulse.
j_i	= ion current density.
L	= plasma discharge chamber length.
\dot{m}	= propellant mass flow rate.

* Assistant Professor, Aerospace Engineering Department, jaume.navarro@uc3m.es

† PhD Student, Aerospace Engineering Department, mwijnen@pa.uc3m.es.

‡ Associate Professor, Aerospace Engineering Department, pablo.fajardo@uc3m.es.

§ Professor, Aerospace Engineering Department, eduardo.ahedo@uc3m.es.

¶ PhD Student & System Engineer, Avionics and Flight Systems, victor.gomez@aeroespacial.sener.

|| RF Design Engineer, Avionics and Flight Systems, alvaro.gimenez@aeroespacial.sener.

** Project Manager, Avionics and Flight Systems, mercedes.ruiz@aeroespacial.sener.

n	= Plasma density.
P_a	= absorbed power.
P_{RF}	= RF power.
r	= radial distance between the centre of the thruster outlet section and the plasma probe /or chamber radius depending on the context.
T_e	= electron temperature.
η_u	= propellant utilization.
η	= thrust efficiency.

I. Introduction

THE Helicon Plasma Thruster (HPT)¹⁻³ had been proposed early in this millennium as a reliable technology for in-Space Electric Propulsion. This concept is essentially based on the use of a Helicon Source^{4,5} to produce a dense plasma and accelerate it supersonically in a second stage, called Magnetic Nozzle (MN), which is mainly a convergent-divergent magnetic field. The neutral gas is ionized and heated by electromagnetic excitation power at the radio-frequency (RF) range, typically 13.56 MHz. Some advantages against other mature devices, such as the Ion Gridded or the Hall Effect Thrusters,⁶ have been underlined by the Electric Propulsion community:⁷⁻⁹ the lack of electrodes, the flexibility in the propellant choice, an expected throttleability (variable thrust and specific impulse) by tuning its operational parameters, and a long lifetime, in principle, thanks to the magnetic screening of its walls.

The EP2 group started the research on this concept with a set of theoretical analyses of the fluid dynamics plasma response at the MN or external flow¹⁰ and within the helicon source.¹¹ A preliminary work performed by Martinez *et al.*,¹² based on the formulation of Cho *et al.*,¹³ inquired into the analysis of the plasma-wave phenomena, following a one-dimensional approach. This work on plasma-wave interaction was extended later into a 2D formulation by Gómez and Navarro-Cavallé *et al.*¹⁴ based on the model of Chen *et al.*¹⁵ Later on, theoretical and numerical analyses were extended by the consortium within the frame of an ESA-TRP project. This would be considered as the kick-off for the design of the first experimental platform, rated at 1 kW, the so called HPT05 prototype,¹⁶ which, for instance, presented very poor performances,¹⁷ as a discouraging propellant utilization below 1 %. A modified version of the original prototype showed a significant increase of the propellant utilization^{18,19} close to 20 %. Further details on the different milestones reached by the UC3M-SenerAeroespacial consortium in the development of the different HPT prototypes will be summarized in Section II. For each one, the main characteristics of their architectures will be reviewed and linked to their propulsive performances, whenever possible. Recently, within the frame of an ESA-GSTP project, the HPT05M prototype has been intensively tested showing an outstanding improvement of its performances: almost full propellant utilization for Xenon at 450 W and a thrust efficiency above 10 %. The details on the implemented experimental methodology to derive the mentioned propulsive performances for both Argon and Xenon as the propellant will be given in Section III. In section IV the pre-design of the HPT03 prototype will be disclosed. This is an engineering model of the thruster unit and the radiofrequency generator and processing unit (RFGPU) developed in the frame of a GSTP-ESA project. The last section wraps up the conclusions of this work.

II. HPT development

The HPT05 prototype (see Figure 1) was designed to operate in the 0.5-1.5 kW (@7.78, 13.56 and 27.12 MHz) power range,¹⁶ although most of the tests were carried out below 1 kW.¹⁷ It was designed to be fed with Argon, as the usual gas for experimental research at that initial phases of development. The nominal mass flow rate was set at 1.5 mg/s of Argon. The magnetic generator was based on a couple of solenoids in a Helmholtz-like configuration, to generate an almost uniform axial field at the plasma source region, plus a third coil aim to generate and tune the MN stage. The maximum magnetic field strength, quite uniform in between the Helmholtz topology was set at 600 G. The plasma discharge chamber consisted of a quartz tube, 30 mm in diameter, and a maximum operating length about 250 mm (nominal at 150 mm), thus being the length adjusted by moving the injector for/backward. The moveable injector was made of



Figure 1. Left: CAD draw of the HPT05 prototype [Ref. 16]. Right: HPT05 prototype under testing at Corona vacuum chamber, ESA-ESTEC [Ref. 17].

Macor®). The RF half-turn helical antenna, 75 mm length, was placed in between the pair of solenoids. The antenna was fed by a balanced feeder. At the other side of the feeder, a π – type matching network was in charge of matching the antenna-plasma impedance to the 50 Ohm characteristic output impedance of the customized off-the-shelf (COTS) power amplifier (PA).

In its first test, performed at ESA-ESTEC facilities,¹⁷ only the propellant utilization, $\eta_u = \dot{m}_i/\dot{m}$, was measured by sweeping an array of 9 Faraday probes (FP) mounted on a semi-circular arm. This magnitude was very low, $\eta_u \lesssim 1\%$, within a wide range of power and mass flow rates, $P_{RF} \in 300\text{-}600$ W and $\dot{m} \in 1.19\text{-}1.78$ mg/s respectively. The feasible explanation to those poor results was attributed to the inefficiency of the RFGPU, concluding that most of the RF power delivered by the PA did not reach the antenna, and was lost mainly at the feeder and matching network circuitry.

Later on, the HPT05-RFGPU subsystem was slightly modified, but keeping the same geometric parameters for the thruster unit (see Figure 2 top), i.e. the same magnetic field generator, chamber sizes and the injector. The helical antenna was temporarily replaced by a simple double loop antenna, made of copper and fed by a coaxial feeder. For this configuration, both the matching network and the PA were COTS components. These modifications had an important impact on the increase of propulsive efficiencies as reported in Ref. 18, 19. A parametric analysis of the increase of η_u with P_{RF} was performed (at 50 sccm of Argon, and a fixed magnetic topology), obtaining that η_u increases from 10 % at 400 W, up to 19 % at 900 W (bottom left plot of Fig. 2). After that, special attention was invested to identify the magnetic topology that drive the HPT05 to the best performances, say increase the ion beam current, I_b . The best result concerning I_b was obtained when the field generated by the back solenoid (S1 feed with -5.3 Amp) opposes that of the two other coils (S2 at 12 Amp and S3 at 16 Amp), thus producing a separatrix (a region of nearly null magnetic field) between the solenoids S1 and S2. This configuration is considered as the nominal magnetic field topology for the HPT05 modified prototype. The ion current density profiles j_i were measured at the plasma beam, and after normalization, it was checked that for the HPT05 modified prototype, the increase of power did not play any role in the ion beam structure (bottom right plot of Fig. 2). The role of the MN on the beam collimation was also proven, by turning off S3 coil, the divergence of beam increased dramatically. Finally, the double loop antenna was supposed to be the main responsible of the formation of a double peak beam structure, the usual shape for inductively coupled helicon plasmas.

Apart from the measurement of η_u , for the HPT05 modified prototype, axial profiles of main plasma properties along the plasma beam axis line were recorded. Plasma densities about 10^{18} m^{-3} were measured at the source exit, for the nominal magnetic configuration, $\dot{m}_{Ar} > 50$ sccm and $P_{RF} = 800$ W. Electron temperature increased up to 6 eV at mass flow rates below 50 sccm of Argon (for the same RF power) and it kept almost constant at about 4 eV for the full mass flow range $\dot{m} = 60 - 100$ sccm.

The last update on the HPT experimental research yield the HPT05M prototype, Figure 3. Several major modifications of different subsystems or components have been implemented. At thruster unit, Macor and quartz plasma discharge chambers have been tested, and also for two different internal diameters, $D = 20$ and $D = 25$ mm. The magnetic field generator has been reduced to the use of a single solenoid (S2 at the original position of S3, MN coil). The antenna has been replaced again by the a half-turn helical antenna.

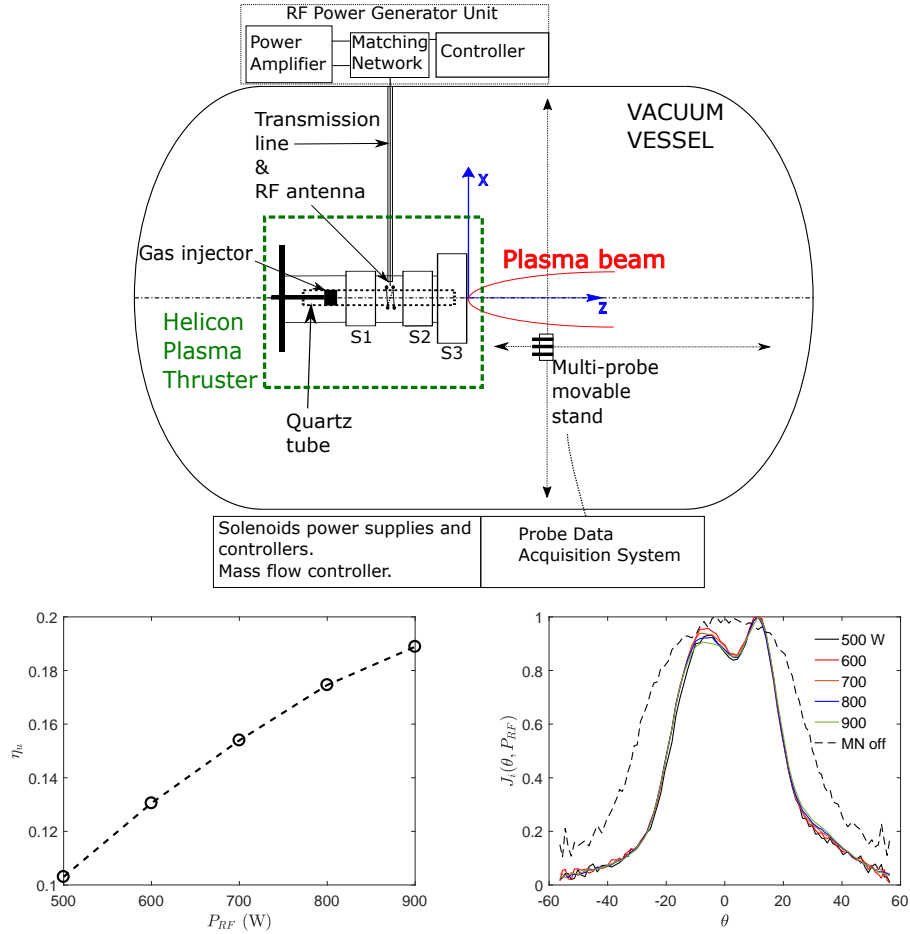


Figure 2. Modified HPT05 prototype [Source Ref. 19]. Top: Sketch of the HPT05 experimental setup at UC3M premises. Bottom left: $\eta_u(P_{RF})$ at 50 sccm of Argon, and nominal magnetic configuration. Bottom right: Ion current density j_i normalized profiles, measured at the HPT05 plume at different power levels and 50 sccm, and nominal magnetic configuration. Comparison against the case of null MN field (dashed line).

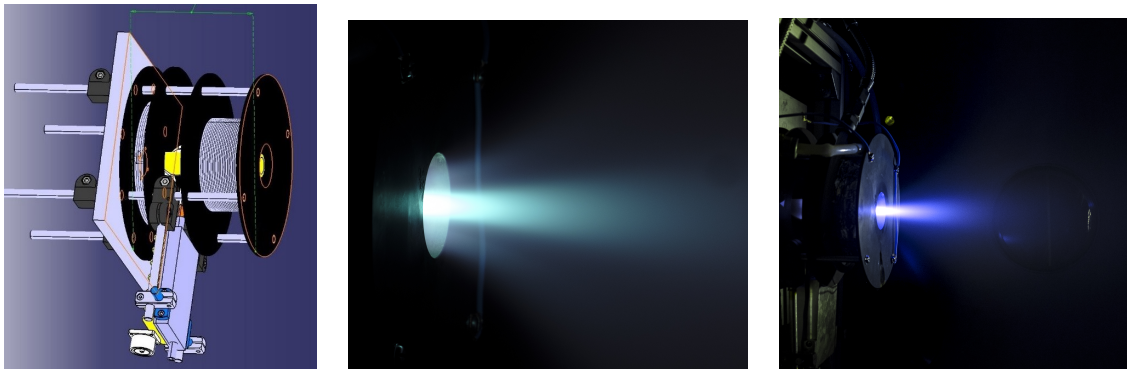


Figure 3. HPT5M prototype CAD draw (left) firing at 10 sccm of Xenon (centre) and 20 sccm of Argon (right), at 1500 G, and 450 W. The plasma beam is extremely well collimated.

A variable π – type matching network outside of the vacuum chamber aims to match the antenna-plasma impedance. Regarding the PA, for most of the tests the former COTS-PA was used, but a PA designed by SENER was tested lately 2018 during a coupling test with the HPT05M thruster unit, validating in this way, the achievement of TRL4 for the full propulsive system. Mass flow rates have been reduced down, 10-20 sccm for Argon, as the nominal range, and 5-10 sccm for Xenon. The effect of the magnetic field strength has been analysed roughly in the 600 to 1500 G range. The nominal PA output power has been set to 450 W, although some performances have been explored beyond that power, up to 600 W, and also down to 300 W. For this prototype a large amount of data concerning the properties and structure of the plasma beam have been acquired, which allows to assess more coherently the thruster performances. An issue that will be deeply discussed in the next section. Recently, the solenoid of the HPT05M prototype has been replaced by an arrangement of permanent magnets, and preliminary measurements have been obtained. However, these are not reported in this work because more data has to be acquired to assess the quality of the obtained results. The series of experiments on the permanent magnet version of the HPT05M are providing nowadays the required inputs for the design of the HPT engineering model, the HPT03 prototype, which will be described in Section IV.

III. Methodology for the assessment of the HPT propulsive performances. Results for the HPT05M prototype.

For the HPT05M, different operating configurations have been tested: combining different mass flow rates, magnetic field strength, and power levels, and even different chamber materials as aforementioned. Nevertheless, in some setup configurations and due to testing time limitations, only some measurements were taken and not a complete scan of all the variables. The plasma properties that have been measured for most of the operating scenarios and configurations are listed next:

- Propellant utilization (η_u), ion beam current (I_B), and plume divergence (α_d), all of them estimated from the ion beam current density profiles $j_i(\alpha)$ measured by a Faraday Probe (FP).
- Plasma density n , plasma potential ϕ and electron temperature T_e are measured by means of a RF compensated Langmuir Probe (RFCLP), after postprocessing accurately the acquired characteristic $I - V$ curves.
- The ion energy distribution function (IEDF), measured by means of a Retarded Potential Analyzer (RPA).

All the commented intrusive plasma diagnostics are mounted on a rotary arm system, that allows to scan the plasma properties in a 2D horizontal plane that contains the thruster axis. The arm centre of rotation is aligned with the centre of the thruster outlet section. r is the distance between this centre and the probe collecting surface. Probes can be moved along this r distance from 0 to 450 mm. Azimuthally, probes can be moved from $\alpha = -90, +90$.

The propellant utilization η_u is computed as usual,

$$\eta_u = \frac{I_b}{e\dot{m}}, \text{ with,} \quad (1)$$

$$I_b = \int_{\alpha} j_i \sin(\alpha) \cos(\alpha) \pi r^2 d\alpha. \quad (2)$$

For all FP scans, j_i is measured in the range $\alpha \in [-70, +70]$ deg, with a resolution of $\Delta\alpha = 2.5$ deg for $\alpha \in [-20, +20]$ and 5 deg for the rest of angles. Because the full $\alpha \in [-90, +90]$ is not scanned by the FP, the usual definition of α_d based on the swept angle that contains a certain % of I_b does not apply neither. So, the authors decide to use another definition based on the azimuthal half angle of half maximum current, $\alpha_d = \alpha(j_{i,max}/2)$.

Based on the data acquired by each probe, and by adding the required assumptions whenever necessary, some propulsive performances can be addressed, such as the thrust F , the specific impulse I_{sp} , and the thrust efficiency η . Specifically, thrust is derived from direct measurements of the ion beam energy (IEDF), combined with the ion density current $j_i(\alpha)$, and complemented by some Langmuir probe measurements. The IEDF is obtained at constant radial position but only at a given set of discrete azimuthal positions, i.e.

$\alpha_m = \{-40, -20, -10, 0, 10, 20, 40\}$ deg. At angles beyond ± 40 deg the RPA measurements are quite noisy since $j_i(\alpha)$ decays abruptly at the beam periphery. The mean ion kinetic energy, \bar{E}_i , is computed from the IEDF, $f_i(E_i)$ and it is the value considered for thrust estimation:

$$\bar{E}_i = \frac{\int E_i f_i dE_i}{\int f_i dE_i}. \quad (3)$$

The combination of $j_i(\alpha)$ with \bar{E}_i allows for the estimation of the ion kinetic energy flux, $e_i = j_i \bar{E}_i$ (energy flux in W/m² if E_i is given in Volts) at the positions in which the RPA measurements are available. A Gauss fitting is performed on the set of discrete point of $e_i(\alpha_m)$ with $m = \alpha_1, \alpha_2, \dots, \alpha_n, \dots$ and the ion energy flux function $e_i(\alpha)$ is obtained and extrapolated from ± 40 to ± 70 deg. $e_i(\alpha)$ is projected into the axial direction and integrated over the spherical shell, from $\alpha = -70$ to $\alpha = +70$ in order to assess the ion beam axial kinetic power, P_{iz} :

$$P_{iz} = \int_{\alpha} e_i \cos(\alpha) \sin(\alpha) \pi r^2 d\alpha. \quad (4)$$

This computation implicitly assumes, as well as in the computation of I_b (Eq. 2), the axial symmetry of the plasma beam and this expression is averaging measurements at α with the corresponding measurement at each symmetric position $-\alpha$. Then, the thrust efficiency, according to its classical definition, $\eta = P_{iz}/P_a$, can be easily assessed by relating P_{iz} with the corresponding plasma absorbed power, P_a . In all the results presented in this document, $P_a = 0.75 P_{RF}$ is considered, which is a conservative assumption of the actual power coupled to the plasma. Conservative in the sense of η , meaning that the actual power coupled effectively to the plasma is presumably lower. Furthermore, P_{iz} is computed from measurements taken at a certain plume position in which the beam is not fully expanded, i.e. there is still an important amount of internal energy that might be effectively transformed into ion kinetic energy. As a result, if P_{iz} is considered alone, it leads to an underestimation of thrust performances.

Let's open a break in the methodology to remind the reader about the ion acceleration mechanism within an HPT device, or specifically, along its MN stage. The energy coupled to the plasma within the HPT source is mainly stored in the shape of thermal electron energy. As a crude approach, electrons expands outwardly, along the MN, as if it were an ideal hot gas in a common divergent nozzle. One of the main differences is that this electron expanding cloud, or each one of the electrons that form the cloud, are well magnetized. Then, they follow the magnetic field lines, so their trajectories are "restricted" by the field. This electron cloud expansion is also conditioned by the presence of ion particles. These are heavier and un-magnetized. Because the large difference between ion and electron dynamics, an ambipolar field arises to keep them together, and avoid charge separation, in other words, the electrons react to the presence of ions, establishing an electric field that pull the ions out. At momentum equation level, the ambipolar field balances the electron pressure, and the ambipolar field balances the ion momentum gain. Concluding that there is a transformation, at energy level, from electron thermal energy to ion kinetic energy.

According to this ion acceleration mechanism, the residual energy is in principle stored in the shape of electron pressure. RFCLP data provides information about the plasma potential, plasma density and temperature at the same position of RPA measurements. This would allow including the pressure term contribution to thrust, or the internal energy of electrons contribution to beam energy. Another way to analyse the remaining electron energy is to infer it from the work that the electric field would do to expand the plasma from the measured plasma potential to 0 (far downstream, or the chamber ground in the lab experiment). However, the uncertainty on the plasma density/potential measurements along an expanding magnetized plasma is still large in most of the literature. Taking this density/potential measurement to assess the plasma pressure contribution to thrust usually leads to an overestimation of thrust. Nevertheless, it has been checked that this term is of the same order of the "extrapolated" plasma pressure at the HPT05M outlet $n_0 T_{e0}$, concluding that this approach to indirectly estimate HPT05M thrust is a reasonable, feasible and conservative method.

Finally, after computing the thrust efficiency and accounting for the known operating mass flow rate \dot{m} operating point, thrust and specific impulse figures can be derived as,

$$\eta = \frac{F^2}{2\dot{m}P_a}, \quad (5)$$

$$I_{sp} = \frac{F}{\dot{m}}. \quad (6)$$

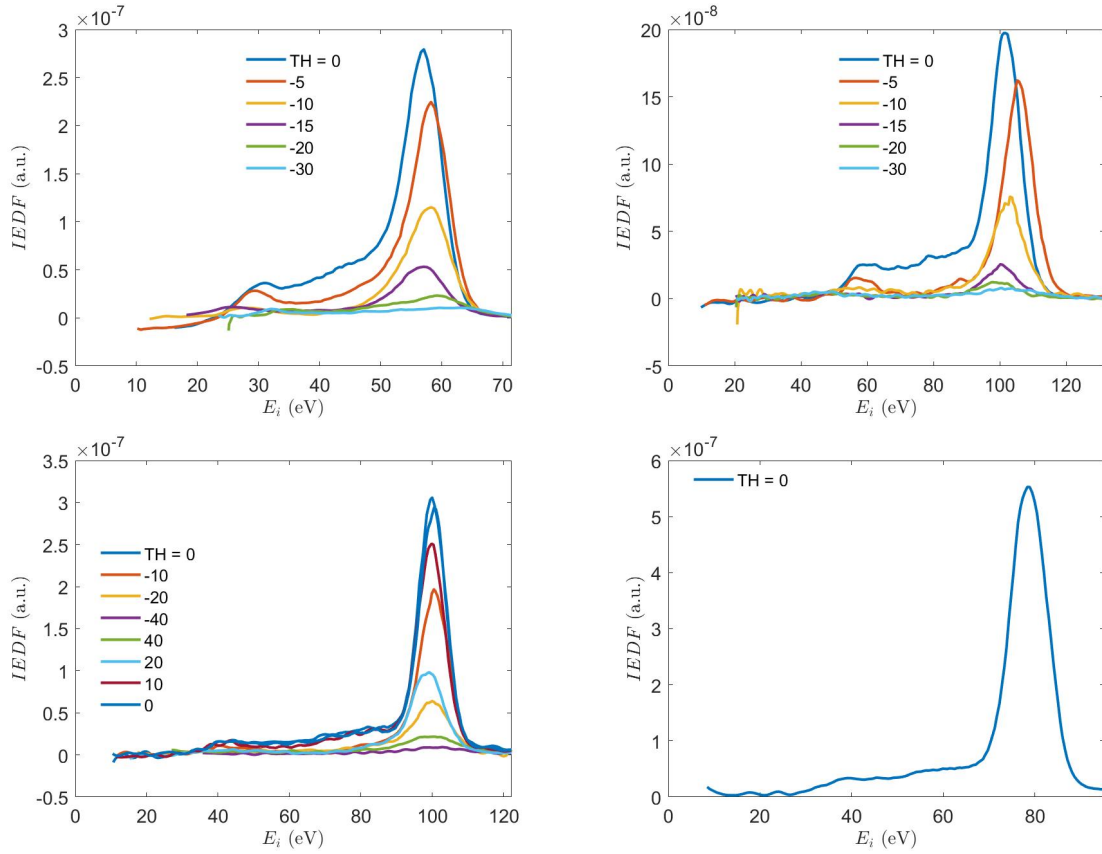


Figure 4. IEDFs for Xenon (1500 G, top left 10 sccm, top right 5 sccm) and Argon (20 sccm of Ar, bottom left 1500 G and bottom right 1000 G). HPT05M with a quartz chamber of $D = 25$ mm, half-turn helical antenna, operating at $P_{RF} = 400$ W.

Next, the described methodology is applied to one of the HPT05M configurations. A version of the prototype implementing a quartz tube, 25 mm and 150 mm in diameter and length respectively. PA delivers the nominal power $P_{RF} = 450$ W, thus $P_a = 337.5$ W will be taken.

As the first step of the methodology, in Figure 4 the measured IEDFs are presented, for both Xenon and Argon. For Xenon, two mass flow rates, 5 and 10 sccm, are analysed, while the magnetic field B is set at 1500 G. For Argon, \dot{m} is set at 20 sccm, while two different magnetic strengths are investigated, 1000 and 1500 G. IEDFs are measured at $r = 300 - 400$ mm and at some discrete azimuthal positions. The ion energy of maximum probability, $E_{i,M}$, rises by decreasing \dot{m} , as shown in the Xenon IEDF results (Figure 4). For Argon, although this behaviour is not reported in this document, it has been checked that $E_{i,M}$ also increases when \dot{m} is reduced. For Argon scenarios, it can be checked that $E_{i,M}$ slightly rises by increasing B . In the Argon test at 1500 G, a small asymmetry on the IEDF measurements can be seen.

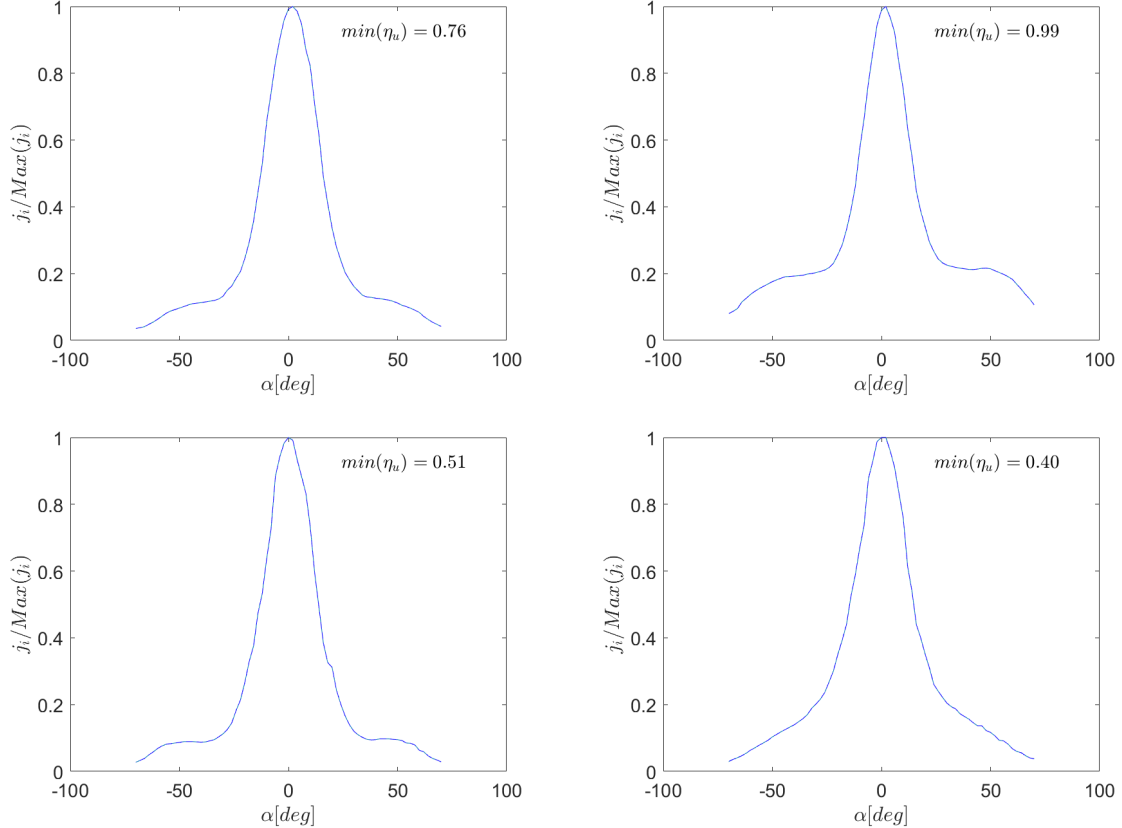


Figure 5. Normalized ion current density profiles for Xenon (1500 G, top left 10 sccm, top right 5 sccm) and Argon (20 sccm of Ar, bottom left 1500 G and bottom right 1000 G). HPT05M with a quartz chamber of $D = 25$ mm, half-turn helical antenna, operating at $P_{RF} = 400$ W.

In Figure 5, the normalized ion current density profiles, $\hat{j}_i(\alpha)$ are depicted for the same operating points as in the IEDF analysis. Each curve is normalized by its maximum current, $j_{i,max}$ and each plot is accompanied by the η_u result. This presents a nearly full ionization at 5 sccm of Xenon, about 70 % at 10 sccm of Xenon, over 50 % at 20 sccm of Argon (1500 G), and 40 % for the same \dot{m}_{Ar} but at 1000 G. This result verifies the lower cost of ionization for Xenon in comparison to Argon, a result that is expected based on the lowest ionization energy threshold for Xenon. Profiles for Xenon present a lateral wings at ± 50 deg. The prominence of these lateral structures has been analyzed for other purposes of HPT research, and it has been checked that bumps are related mainly to the plasma magnetization effectiveness. The higher magnetization (in the sense of magnetic confinement vs perpendicular transport) the stronger these structures. Thus, for the low mass flow rate scenario, it corresponds to a lower collisionality, that impacts on the increase of these structures. This effect appears as well in the Argon scenarios. It can be checked how for the 1000 G case, the lateral wings do not exist and the lateral bumps appear again at 1500 G. The stronger magnetic field confines better the generated plasma further away from the lateral walls of the quartz tube, and these structures

are transported downstream where the FP data is acquired. When the magnetic field is reduced, plasma interacts more with the quartz tube and this structures vanish, penalizing deeply on the η_u result. Indeed, a lost of 10 % when B is reduced from 1500 to 1000 G.

j_i and E_i are combined at the points in which the IEDF is measured to get the ion kinetic energy flux, e_i . A Gaussian fitting is applied to the discrete measures. These results are presented in Figure 6 for the same scenarios as before. For the sack of compactness, the step-by-step procedure to get e_i is not detailed, but for some cases, in which there is lack of data concerning the IEDF measurements at some angles, it is evident that more hypotheses and simplifications have been taken.

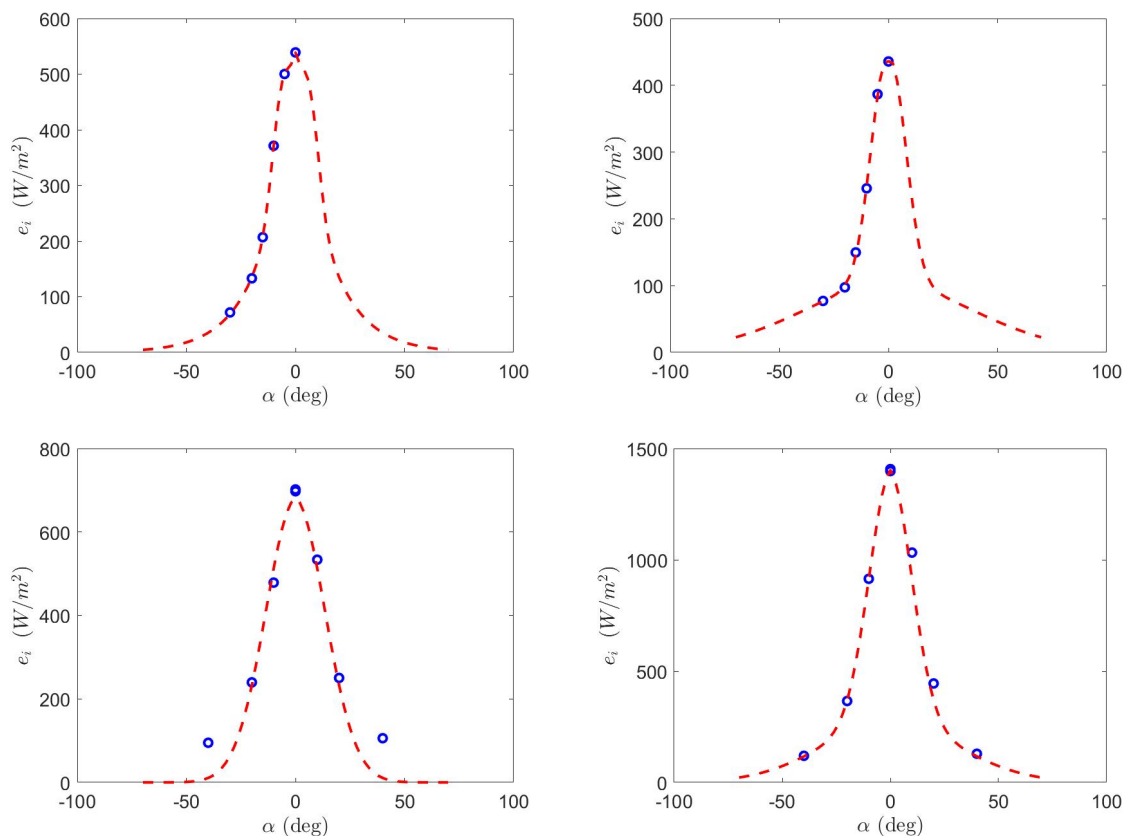


Figure 6. Ion kinetic energy flux fitted profiles, $e_i(\alpha)$ for Xenon (1500 G, top left 10 sccm, top right 5 sccm) and Argon (20 sccm of Ar, bottom left 1500 G and bottom right 1000 G). HPT05M with a quartz chamber of $D = 25$ mm, half-turn helical antenna, operating at $P_{RF} = 400$ W.

After presenting all these partial results on f_i , j_i and e_i , the rest of the methodology presented above can be applied. The obtained results concerning thrust, thrust efficiency, specific impulse and beam divergence are summarized in Table 2. For the estimation of the amount of residual internal energy stored within the plasma at the place where probe measurement are taken, the two methods commented above are considered, and the most conservative result in terms of η is taken.

\dot{m} (sccm)	η_u (%)	η (%)	F (mN)	I_{sp} (s)	α_d (deg)
10 Xe	98-99	7.7-10.53	5.2-6.1	1027-1212	12
5 Xe	70-77	8.46-9.71	7.6-8.2	762-815	13
20 Ar	51	14.2	7.6-9.4	1297-1613	12-14
20 Ar(*)	40	12.1	7-7.5	1196-1288	12-14

Table 2. Summary of thrust performances for the HPT05M prototype. Nominal power 450 W, and nominal magnetic strength 1500 G. (*)1000 G.

In terms of propellant utilization, the prototype behave as expected, and the use of Xenon allows to reach

a very high utilization, close to full ionization, $\sim 100\%$ at 5 sccm of Xe, while it drops down to 50 % for 20 sccm of Argon, for the same power, 450 W, and magnetic field strength about 1500 G. However, from the point of view of achieving a higher (thrust) efficiency there are more aspects that must be considered.

Before moving ahead with other issues, let analyze which is the real meaning of the measured propellant utilization. It is evident that the decrease in mass allows to increase this efficiency. However, in terms of ejected ions the decrease in mass, or changing from Xenon to Argon, could imply in both cases a descent of the ion density. So it is important to clarify the cases that have been compared. For example, at 5 sccm of Xe (0.46 g/s, equivalent to 2.24×10^{18} part/s), assuming a conservative utilization of 95 %, this is equivalent to an ion particle flow rate of 2.13×10^{18} part/s, while at 20 sccm of Ar (0.59 g/s, equivalent to 8.96×10^{18} part/s), assuming an utilization of 50 %, this is equivalent to a particle flow rate of 4.48×10^{18} part/s. The mass flow rate of Argon (20 sccm) is a 22 % larger than that of Xenon (5 sccm), however, accounting for the respective utilization, the mass utilization for argon is a 36 % lower than that of Xenon, but in terms of ejected particles, the Argon case is still ejecting double of the particles of the Xenon case, and at a higher velocity.

Taking into account these numbers, it seems that the equivalence between Ar and Xe is not fair in terms of mass flow rate. This comparison can be easily explained and understood. Furthermore, the use of different propellants has an impact on other properties, such as a big difference on collisional processes, which at the end, determine or play one of the most important roles in the energy balance. From this balance, the plasma will reach different temperatures, and this makes to establish a different acceleration electric field. Different fields yield to different velocities of the ejected particles, and consequently this impacts directly on thrust and beam energy. But in the determination of this thrust the particle density is an important factor as well, and the circle is closed. To sum up, the reader should keep in mind that plasma is a self-organized process, in which particle interaction is the main mechanism to transport mass, momentum and energy, so, the overall response depends on how this complex mechanism behaves to the imposition of boundary constraints. If the nature and number of particles is different, it is obvious that to establish a parallelism between them is a tough issue, but affordable if the differences on the particle-interaction character are roughly known.

For Xenon, the table reveals a double mode of operation, a low thrust high specific impulse at 5 sccm, and higher thrust but at lower specific impulse at 10 sccm. This double mode is justified by the different particle-energy balance of each case. At 5 sccm, the number density is lower, this decreases “inelastic” collisional processes. Consequently, electrons reach a higher temperature, and ions gain more energy along the expansion, and as a result higher velocities. However, this higher velocity is strongly penalized by the lower density number in the computation of thrust. At 10 sccm, the higher collisionality penalizes on the electron temperature, ions are accelerated to lower velocities, penalizing dramatically on the specific impulse. Nevertheless, the thrust is kept high thanks to a higher particle density. The case that it seems more competitive is the one of Argon at 20 sccm. Although the utilization is low, the total number of particles is higher and their velocities larger as well. This high velocity, although the electron temperature is not necessarily as high as in the Xenon case (5 sccm), is reached because of the lower mass of Argon ions. Finally, both gases present similar plasma plume divergences. This means that the divergence is established by the electrons confinement and other processes regardless of the gas kind.

IV. Predesign of the HPT03 engineering model

Based on the results and knowledge acquired thanks to the intense experimental research on the HPT05M and previous prototypes, the predesign of the first engineering model has been set. This engineering activity is mainly focused on the thruster unit, including also the RF antenna design. Concerning the magnetic generator, it is one of the major modifications, being the solenoid replaced by an arrangement of permanent magnets. The magnetic field topology cannot be disclosed yet. The plasma discharge chamber will be more compact than that of the HPT05M breadboard. It will be made of ceramic material, choosing the best among the existent options, giving priority to flight qualified materials, and accounting for its mechanical and thermal properties and electromagnetic compatibility. In terms of operating parameters, it will be rated at 450 W of maximum RF power, magnetic field strengths in the order of 1000 G, and mass flow rates of Xenon about 10 sccm. The expected HPT03 mass budget is below 5 kg for the thruster unit, and below 13 kg overall (including both the power generation unit and the thruster unit). The expected dimensions are within the envelope defined as 115*182*139 mm. The HPT03 unit is expected to be operated as a plug and play unit. A preliminary CAD draw of this model is depicted in Figure 7.

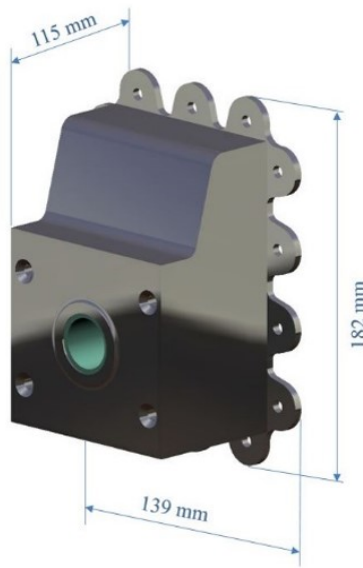


Figure 7. CAD draw of the HPT03 engineering model.

V. Conclusions

This work has reviewed the experimental research on HPT technology for Space Missions, carried out by the UC3M - SENER Aerospace consortium during the last 3-4 years. The methodology to assess HPT thrust performances by scanning the plasma plume properties using intrusive probes has been presented. This methodology has been applied to the real case of the HPT05M prototype operating with both Xenon or Argon, at a nominal power of 450 W and a magnetic field strength about 1500 G (convergent-divergent topology). Thrust efficiency about 10 % has been estimated, indicating that the HPT05M platform is close or above the current HPT state-of-the-art. Finally, a brief description of the new engineering model has been included to disclose the next steps of the consortium on the design of reliable and feasible HPT for Space Missions.

Acknowledgments

This work has been partially supported by Project ESP2016-75887 (Spain's National Research and Development Plan - MINECO/FEDER). Additional funds come from the GSTP-ESA project No.4000125311/18/NL/KML/va, "Improvements in Helicon Plasma Thruster (HPT) for its evolution towards Space application".

References

- ¹Charles, C. and Boswell, R., "Current-free double-layer formation in a high-density helicon discharge," *Applied Physics Letters*, Vol. 82, No. 9, 2003, pp. 1356–1358.
- ²Batishchev, O., "Minihelicon Plasma Thruster," *IEEE Transaction on Plasma Science*, Vol. 37, 2009, pp. 1563–1571.
- ³Pavarin, D., Ferri, F., Manente, M., Lucca Fabris, A., and Trezzolani, F., "Thruster Development Set-up for the Helicon Plasma Hydrazine Combined Micro Research Project (HPH.com)," *32nd International Electric Propulsion Conference, Wiesbaden, Germany*, Vol. IEPC-2011-241, 2011.
- ⁴Boswell, R., "Very efficient plasma generation by whistler waves near the lower hybrid frequency," *Plasma Physics and Controlled Fusion*, Vol. 26, 1984, pp. 1147–1162.
- ⁵Chen, F., "Plasma ionization by helicon waves," *Plasma Physics and Controlled Fusion*, Vol. 33, 1991, pp. 339.
- ⁶Goebel, D. and Katz, I., *Fundamentals of electric propulsion: ion and Hall thrusters*, John Wiley & Sons Inc, 2008.
- ⁷Charles, C., Boswell, R., and Lieberman, M., "Xenon ion beam characterization in a helicon double layer thruster," *Applied Physics Letters*, Vol. 89, 2006, pp. 261503.
- ⁸Takahashi, K., Laffeur, T., Charles, C., Alexander, P., and Boswell, R., "Electron Diamagnetic Effect on Axial Force in an Expanding Plasma: Experiments and Theory," *Physical Review Letters*, Vol. 107, No. 23, 2011, pp. 235001.

- ⁹Little, J. M. and Choueiri, E. Y., “Critical Condition for Plasma Confinement in the Source of a Magnetic Nozzle Flow,” *IEEE Transactions on Plasma Science*, Vol. 43, No. 1, 2015, pp. 277–286.
- ¹⁰Ahedo, E. and Merino, M., “Two-dimensional supersonic plasma acceleration in a magnetic nozzle,” *Physics of Plasmas*, Vol. 17, 2010, pp. 073501.
- ¹¹Ahedo, E. and Navarro-Cavalle, J., “Helicon thruster plasma modeling: Two-dimensional fluid-dynamics and propulsive performances,” *Physics of Plasmas*, Vol. 20, 2013, pp. 043512.
- ¹²Martinez, D. and Ahedo, E., “Plasma-wave interaction in a helicon thruster,” *32th International Electric Propulsion Conference, IEPC-2011-047 (Electric Rocket Propulsion Society, Fairview Park, OH, 2011)*, 2011.
- ¹³Cho, S. and Lieberman, M., “Self-consistent discharge characteristics of collisional helicon plasmas,” *Physics of Plasmas*, Vol. 10, 2003, pp. 882–890.
- ¹⁴Navarro-Cavallé, J., Merino, M., Ahedo, E., Gómez, V., and Ruiz, M., “Helicon Plasma Thrusters: prototypes and advances on modeling,” *33th International Electric Propulsion Conference, IEPC-2013-285 (Electric Rocket Propulsion Society, Fairview Park, OH, 2013)*, 2013.
- ¹⁵Chen, G., Arefiev, A., Bengtson, R., Breizman, B., Lee, C., and Raja, L., “Resonant power absorption in helicon plasma sources,” *Physics of plasmas*, Vol. 13, 2006, pp. 123507.
- ¹⁶Merino, M., Navarro-Cavallé, J., Casado, S., Ahedo, E., Gómez, V., Ruiz, M., Bosch, E., and del Amo, J. A. G., “Design and development of a 1 kW-class helicon antenna thruster,” *34th International Electric Propulsion Conference, IEPC-2015-297 (Electric Rocket Propulsion Society, Fairview Park, OH, 2015)*, 2015.
- ¹⁷Merino, M., Navarro-Cavallé, J., Ahedo, E., Gómez, V., Sánchez, V., Ruiz, M., Dannenmayer, K., Bosch, E., and del Amo, J. A. G., “Maiden tests of the HPT05 Helicon Plasma Thruster Prototype,” *Space Propulsion Conference 2016*, Association Aéronautique et Astronautique de France, Rome, Italy, 2016.
- ¹⁸Navarro-Cavallé, J., Wijnen, M., Fajardo, P., Merino, M., Ahedo, E., Ruiz, M., and Gómez, V., “Experimental performances of a 1 kW HPT by means of plasma diagnostics,” *35th International Electric Propulsion Conference, IEPC-2017-447 (Electric Rocket Propulsion Society, Fairview Park, OH, 2017)*, 2017.
- ¹⁹Navarro-Cavallé, J., Wijnen, M., Fajardo, P., and Ahedo, E., “Experimental characterization of a 1 kW helicon plasma thruster,” *Vacuum*, Vol. 149, 2018, pp. 69–73.